2018-01-1250 Published 03 Apr 2018

Symmetric Negative Valve Overlap Effects on Energy Distribution of a Single Cylinder HCCI Engine

Khashayar Ebrahimi and Charles Koch University of Alberta

Citation: Ebrahimi, K. and Koch, C., "Symmetric Negative Valve Overlap Effects on Energy Distribution of a Single Cylinder HCCI Engine," SAE Technical Paper 2018-01-1250, 2018, doi:10.4271/2018-01-1250.

Abstract

The effects of Variable Valve Timing (VVT) on Homogeneous Charge Compression Ignition (HCCI) engine energy distribution and waste heat recovery are investigated using a fully flexible Electromagnetic Variable Valve Timing (EVVT) system. The experiment is carried out in a single cylinder, 657 cc, port fuel injection engine fueled with n-heptane. Exergy analysis is performed to understand the relative contribution of different loss mechanisms in HCCI engines and how VVT changes these contributions. It is found that HCCI engine brake thermal efficiency, the Combined Heat and Power (CHP) power to heat ratio, the first and the second law efficiencies are improved with proper valve timing. Further analysis is performed by applying the first and second law of thermodynamics to compare HCCI energy and exergy distribution to Spark Ignition (SI) combustion using Primary Reference Fuel (PRF). HCCI demonstrates higher fuel efficiency and power to heat and energy loss ratios compared to SI. The results are applicable for the development of micro-CHP systems using an HCCI engine operating at a constant engine speed with varying loads.

Introduction

Micro CHP is an effective technology for generating heat and electricity in residential buildings [1]. This technology can replace the conventional heating boilers to provide heat and hot water and the majority of the building electricity [2]. Micro CHP plants are mainly used in countries that have high electricity prices and where CO_2 emission reduction is of concern [1, 2]. HCCI engines present a new opportunity for the micro CHP market since these engines are fuel efficient and can work with wide variety of fuels including natural gas and bio-fuels [3]. HCCI engine design can be optimized for fuel efficiency at specific loads and speeds for micro CHP application. HCCI exhaust emissions are another factor that must be considered for a micro CHP system integrated with HCCI engines. The major HCCI engine emissions are CO and unburned HC [4] and these emissions can be controlled using different actuators and strategies, such as: VVT [5], oxidation catalyst [6], EGR and fuel Octane number [7].

Existing internal combustion engines micro CHP units generate power in a range of 1-100 kW and are used mainly for residential and commercial buildings [1]. Micro CHP systems can also be integrated with turbines and fuel cells for the power source [1, 8]. Compared to internal combustion engines, fuel cells have a higher efficiency and they do not produce NO_X and particulate matter emissions. CHP units with fuel cells are being tested, mainly in Japan and Germany, but have high capital costs [1]. Turbines are typically used for micro CHP systems with 30-200 kW output which is suitable for commercial buildings [1]. The turbine micro CHP units are slower to start and ramp to full load compared to internal combustion engines [1, 2, 9]. Although the internal combustion engines maintenance costs are higher than comparable gas turbines, the maintenance can be handled by in-house staff or local service organizations [10]. Micro CHP systems with internal combustion engine are currently the most economical due to their lower capital costs [10].

There are relatively few studies on HCCI engine energy distribution and exergy analysis. A summary of these studies is provided next. A crank angle based exergy analysis was performed for a HCCI engine using a multi-zone thermo-kinetic model [11]. Four loss mechanisms for HCCI engines were introduced including combustion irreversibility (16.4%-21.5%), heat loss to exhaust (12.0%-18.7%), heat transfer to the cylinder walls (3.9%-17.1%) and chemical exergy lost due to incomplete combustion (4.7%-37.8%). The model developed in [11] was used to define optimal operating points for a gasoline fueled HCCI engine in [12]. The results showed that exergy losses to the exhaust gas are reduced with delayed combustion timing, however, the exergy losses to the unburned species then increase. The optimal combustion timing was determined using the balance of the exergy losses to the unburned species and the exergy losses to the coolant and exhaust gas. Exergy efficiency sensitivity to the intake pressure and equivalence ratio were also detailed over a wide engine operating range. It was found that late combustion timing with higher fuel equivalence ratios and higher boosted intake pressures are preferred at high loads. For low loads, it was

recommended to keep the fuel equivalence ratio high and gradually reduce the boosted intake manifold pressure to the ambient pressure.

A crank angle based single zone model was developed for the second law analysis of a HCCI engine burning natural gas/DME fuel [13]. The exergy efficiency was improved by an increase in excess air ratios of the DME and the irreversibility decreases with increasing intake temperature. A crank angle based single zone model was developed for HCCI engine second law analysis [14]. It was found that an increase in the inlet charge temperature reduces the maximum pressure, indicated work and entropy generation per cycle. The results also showed that fuel exergy destruction is reduced with increasing engine speed and heat loss to the cylinder walls is reduced. An Ammonia-Water Cogeneration Cycle (AWCC) was used to recover heat from the exhaust gas and cooling water of a HCCI engine in [15]. A crank angle based single zone thermodynamic model was used to show that fuel energy saving ratio can be improved up to 28% using the proposed trigeneration system. A natural gas HCCI engine was turbocharged [16] to improve engine performance characteristics and the engine power generating efficiency was investigated for CHP application. The results indicated that the HCCI engine improves the CHP power generating efficiency and reduces the NO_X emission.

Major parameters affecting first and second law efficiencies of internal combustion engines including HCCI were detailed in [17] and different methods were introduced for improving engine efficiency. The effects of intake pressure boosting and variable valve timing on exergy flows of a HCCI engine were detailed using a physical model [18]. It was found that combustion irreversibility is increased at low loads with positive valve overlap and the combustion irreversibility is decreased by changing from the positive valve overlap to negative valve overlap. Cycle temperature was reduced with positive valve overlap and the energy lost to the cylinder walls and exhaust was reduced. The pumping work was lower with positive valve overlap and the brake thermal efficiency was increased with positive valve overlap at boosted intake pressure. Energy distribution analysis was performed for a HCCI engine and the engine efficiency was compared to a port fuel injection SI and a lean burn SI engine [19]. The analysis indicated that combustion irreversibility increases for lean combustion and the HCCI engine offers only modest efficiency improvements compared to the lean burn SI engine due to reduced burn duration.

Combined first and second law analysis were performed for a HCCI engine working with ethanol and the effects of the intake manifold pressure, ambient temperature, and compressor efficiency on engine exergy efficiency were examined [20]. The results indicated that the first and second law efficiencies are improved by increasing the turbocharger pressure ratio and the efficiencies are reduced when the ambient temperature increases. The exergy analysis indicated that the first and second law efficiencies are more sensitive to the turbocharger pressure ratio compared to the turbocharger compressor efficiency and ambient temperature.

A second law analysis was performed for a HCCI engine based on a single-zone model [21]. Blends of n-heptane and natural gas fuel were used and the exergy analysis indicated that exergy destruction is decreased when the natural gas fraction increases in the fuel blend. The effects of EGR on HCCI combustion were investigated and the results indicated that the chemical exergy of the in-cylinder charge is reduced by increasing the EGR rate. The optimum EGR rate was defined based on exergy analysis for a specific engine operating conditions. First and second law analysis were performed for a system consisting of a turbocharged natural gas HCCI engine, a regenerator and a catalyst in [22]. The effects of intake manifold pressure, ambient temperature, fuel equivalence ratio, engine speed and turbocharger compressor efficiency on system exergy efficiency were investigated. The results indicated that thermal and exergy efficiencies are improved at higher intake pressure, fuel equivalence ratios and engine speeds. Increased ambient temperature had adverse effects on both thermal and exergy efficiencies.

Energy and exergy distributions of HCCI engine were compared to Reactivity Controlled Compression Ignition (RCCI) and conventional diesel combustion in [23] using CFD models coupled with detailed kinetic mechanism. The results indicate that the combustion timing affects the energy distribution of the HCCI and diesel engines. The utilization efficiency of heat transfer and exhaust in RCCI was less affected by the variation of combustion timing. It was found that the heat transfer losses in diesel engine is a strong function of the in-cylinder temperature gradient while for the HCCI and RCCI engines it is mainly related to heat transfer area. HCCI and RCCI combustions demonstrate lower exergy destruction compared to diesel at same load. HCCI shows the highest energy and exergy efficiencies and diesel demonstrates the worst. In [24], a model predictive control strategy was developed based on HCCI exergy distribution. The sources of exergy destruction were determined for a HCCI engine and an optimization algorithm was proposed to find the optimum combustion timing in order to maximize the second law efficiency. Average fuel efficiency improvement of 6.7% was obtained using exergy-based optimal control strategy in simulation.

A CFD model was developed and used to compare Gasoline Compression Ignition (GCI) combustion performance to RCCI in [25]. The comparison was made for 20 bar gross indicated mean effective pressure at 1300 RPM. The results indicate that both combustion strategies have high gross indicated efficiency (~47%) with near zero NO_x emissions. Both combustion strategies were sensitive to fluctuations in EGR, with the GCI being more sensitive than the RCCI strategy. In [26], a full-cycle energy analysis was performed for a single-cylinder research engine undergoing low temperature gasoline combustion with varying NVO auxiliary fueling rate and injection timing. Experiments were performed using a 5-component gasoline surrogate (iso-octane, n-heptane, ethanol, 1-hexene, and toluene). The highest total cycle thermodynamic efficiencies were observed when auxiliary injection timings were early enough to allow sufficient residence time for slow reforming reactions to take place, but late enough to prevent significant fuel spray crevice quench. Thermal efficiency was improved by increasing the fraction of total fuel energy injected during NVO, due to endothermic fuel decomposition by pyrolysis. In [27], effects

of engine speed, intake temperature and fueling rate were investigated experimentally on energy distribution of a one-liter displacement single-cylinder boosted low-temperature HCCI-like GCI engine. The results show that combustion timing affects the engine energy distribution and the ringing intensity.

HCCI combined with VVT actuation is flexible enough to examine the potential of HCCI-CHP systems. VVT has been used for combustion timing control extensively [28, 29, 30] but literature on the effects of VVT on port-fuel injection HCCI engine energy distribution is lacking. The potential for HCCI-CHP has not been well-established in the literature while CI and SI have been [31, 32, 33, 34, 35, 36, 37, 38, 39]. In this study, the effects of VVT on engine energy and exergy distribution are detailed experimentally first. Next, HCCI benefit in fuel efficiency and the potential of maximum work extraction from HCCI is revealed by comparing the HCCI energy and exergy distribution to SI at same injected fuel energies. The important factors that affect energy and exergy distribution are detailed and the CHP first and second law efficiencies for these two different combustion modes are examined. To the authors' knowledge, this is the first time that the effects of SNVO duration on port-fuel injection HCCI engine energy and exergy distribution are detailed experimentally.

Experimental Setup

HCCI experiments with VVT are conducted on a single cylinder Ricardo Hydra Mark III engine equipped with EVVT system [5, 40]. Symmetric Negative Valve Overlap (SNVO) is used as valve timing strategy. In SNVO, the Exhaust Valves Close (EVC) timing is set to a crank angle before the piston reaches Top Dead Center (TDC) in the exhaust stroke and the Intake Valves Open (IVO) timing is set to the same amount, or symmetric, after TDC [30]. With symmetric changes of EVC and IVO timings around TDC, recompression work can be regained as expansion work and the pumping work is minimized. The engine has two port fuel injectors but only one of them is used in this study. Fuel flow rate is measured only on the n-heptane side using a coriolis meter (Pierburg PLU4000). Only n-heptane is used as fuel for this experiment and is injected at 80°C intake temperature which avoids fuel impingement on the intake manifold wall. In-cylinder pressure is measured using a Kistler water-cooled ThermoCOMP (model 6043A60) piezo-electric pressure sensor that is flush mounted in the cylinder head. The engine specifications are listed in Table 1. Extra experiments are performed in Waukesha variable compression ratio Cooperative Fuels Research (CFR) engine [41] with the engine specifications listed in Table 1 to compare SI engine energy and exergy distributions to HCCI. The CFR engine can operate in both HCCI and SI modes and the CFR experiments are performed to reduce the effects of engine and combustion chamber geometry on energy distribution analysis. The CFR engine compression ratio is set to 11.2:1 and experiments were performed at same injected fuel energies and low speed (800 RPM).

TABLE 1 Ricardo and CFR engines specifications [5, 41]

Ricardo Engine	
Parameters	Values
Bore × Stroke [mm]	97 × 88.9
Compression Ratio [–]	13.9
Displacement [cm^3]	653
Connecting Rod Length [mm]	159
CFR engine	
Parameters	Values
Bore × Stroke [mm]	83 × 114
Compression Ratio [–]	variable from 4 to 18
Displacement [cm^3]	612
Connecting Rod Length [mm]	254

TABLE 2 HCCI Operating Conditions

Parameter	**Values**
Engine Speed [rpm]	725-825
T_{Intake} [°C]	80
P_{Intake} [kPa]	88-90
Injected Fuel Energy, $Em_{finj}\left[\frac{kJ}{Cycle}\right]$	0.356-0.495
T_{cool} [°C]	85-90
Octane Number (ON) [–]	0
EVC [bTDC]	–350° - –300°
IVO [bTDC]	300° - 350°
EVO [bTDC]	–180°
IVC [bTDC]	180°

The experimental conditions of the 35 HCCI steady-state points measured in Ricardo engine with VVT are summarized in Table 2. The measurements are done by varying the SNVO duration at several fueling rates while the other engine variables including intake manifold temperature and pressure, engine speed, oil temperature, IVC and EVO timings were kept constant. The CFR engine experimental conditions for comparing SI to HCCI are summarized in Table 3. The CFR engine was run with the throttle partially open for SI experiments to keep the fuel equivalence ratio at stoichiometric conditions ($\lambda = 1.0$), while the HCCI experiments performed at wide open throttle with an intake manifold temperature of 112°C ($\lambda = 2.4$). The ratio of iso-octane to n-heptane (fuel octane number) was changed to control combustion timing and to obtain maximum brake thermal efficiency in HCCI as the CFR engine is not equipped with a EVVT system. The fuel octane number was reduced to 38.7 at constant injected fuel energy in HCCI to advance the combustion timing, however, engine knocking was observed for octane values less than 38.7. For SI combustion, spark timing was varied to control combustion timing control and improve brake thermal efficiency. All SI experiments were performed with iso-octane. For energy and exergy distribution analysis, pressure traces from 200 consecutive engine cycles were recorded every 0.1 CAD for each test and the cycle averaged pressure trace was used for energy distribution analysis. More information can be found in [5, 40, 41] regarding the experiment setups.

TABLE 3 CFR Engine Operating Conditions

CFR Engine - HCCI	
Parameters	Values
Engine Speed [rpm]	790-810
P_{Intake} [kPa]	92-96
T_{Intake} [°C]	110-113
Injected Fuel Energy $\left[\frac{kJ}{Cycle}\right]$	0.65
T_{cool}°C	87-93
Octane Number (ON) [–]	38.5-50.5
CFR Engine - SI	
Parameters	Values
Engine Speed [rpm]	790-810
P_{Intake} [kPa]	61-64
T_{Intake} [°C]	18-20
Injected Fuel Energy $\left[\frac{kJ}{Cycle}\right]$	0.65
T_{cool} [°C]]	90-95
Octane Number (ON) [–]	100
Spark Angle [bTDC]	10-20

Energy and Exergy Analysis

HCCI Energy Distribution Analysis

The injected fuel energy is assumed to follow six different energy pathways in internal combustion engines as shown in Figure 1 and only part of injected fuel energy is turned into the useful work. The first energy pathway is part of the injected fuel energy lost due to incomplete combustion. To calculate how much energy is lost due to incomplete combustion, combustion efficiency is calculated first. Combustion efficiency, η_{Comb} is defined [42] as

$$\eta_{Comb} = \frac{c_1 Q_{HR}}{m_f LHV_f} + c_2 \tag{1}$$

where Q_{HR} is the net energy released during combustion, m_f and LHV_f are the injected fuel mass and fuel low heating value respectively. $c_1 = 55.271$ and $c_2 = 44.176$ are defined using MATLAB Model Based Calibration Toolbox. These constants are parameterized based on the combustion efficiency values calculated in [42] based on measured emissions. The method detailed in [43] is used to calculate combustion efficiency based on measured emissions. The net heat release is then calculated as

$$Q_{HR} = \int_{\theta_1}^{\theta_{99}} \left(\frac{dQ_{HR}}{d\theta}\right) d\theta \tag{2}$$

where θ_1 and θ_{99} are defined as the crank angle for 1% and 99% mass fraction burned respectively. The apparent heat release rate, $\frac{dQ_{HR}}{d\theta}$ is calculated using a single zone model [43] as

$$\frac{dQ_{HR}}{d\theta} = \frac{1}{k-1} V \frac{dP}{d\theta} + \frac{k}{k-1} P \frac{dV}{d\theta} \tag{3}$$

where k, P and V are the specific heat ratio, measured in-cylinder pressure and the in-cylinder volume respectively. The specific heat ratio is calculated analytically using NASA polynomials [44]. A graphical approach [45] is used to define the window limits used to calculate apparent heat release rate. The cylinder volume is calculated at each crank angle from slider crank mechanism equation [43]. The fuel energy lost due to incomplete combustion, Q_{IC} is calculated as

$$Q_{IC} = \left(1 - \eta_{Comb}\right) m_f LHV_f \tag{4}$$

where η_{Comb} is from eqn. 1. Referring to Figure 1, part of injected fuel energy is lost due to pumping work. Pumping work, $W_{Pumping}$ is calculated from the measured cylinder pressure trace as

$$W_{Pumping} = \int_{TDC-Int}^{BDC-Int} PdV + \int_{BDC-Exh}^{TDC-Exh} PdV \tag{5}$$

Next, part of injected fuel energy lost due to friction (see Figure 1) is calculated as

$$W_{friction} = W_{ind} - W_{brake} \tag{6}$$

where $W_{friction}$, W_{ind} and W_{brake} are the friction, indicated and brake work respectively. Brake work, W_{brake} is

$$W_{brake} = 120 \frac{P_{brake}}{\omega} \tag{7}$$

FIGURE 1 Energy balance of internal combustion engines

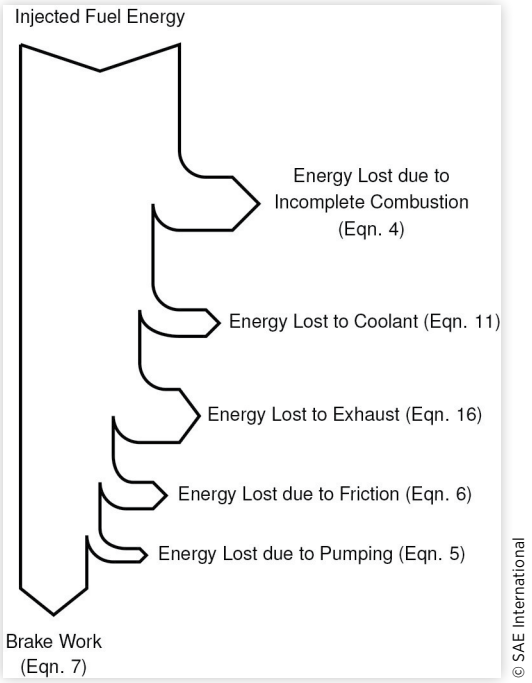

where P_{brake} and ω are brake power and engine speed respectively. Brake power is calculated from the measured engine torque and speed as

$$P_{brake} = \frac{2\pi}{60}\tau\omega \tag{8}$$

where τ is the measured torque. Brake thermal efficiency, $\eta_{th,\,brake}$ represents the fraction of injected fuel energy turned into useful work and is calculated as

$$\eta_{th,brake} = \frac{W_{brake}}{m_f LHV_f} \tag{9}$$

The net indicated work, W_{ind} is calculated from the measured pressure traces as

$$W_{ind} = \oint_{cycle} PdV \tag{10}$$

The amount of injected fuel energy lost due to heat transfer to the coolant, Q_{cool} is calculated as

$$Q_{cool} = \oint_{Cycle} \frac{dQ_{cool}}{d\theta} d\theta \tag{11}$$

where $\frac{dQ_{cool}}{d\theta}$ is the rate of heat transfer to the coolant and is calculated as

$$\frac{dQ_{cool}}{d\theta} = \frac{Ah_c}{\omega}\left(T_{cyl} - T_{wall}\right) \tag{12}$$

where the parameters A, ω, T_{cyl} and T_{wall} are the in-cylinder area exposed to the gas, engine speed, in-cylinder gas temperature and cylinder wall temperature respectively. The wall temperature is assumed to be constant (T_{wall} = 400°K) [46, 47]. The parameter h_c is the heat transfer coefficient and is calculated from the modified Woschni's correlation [48] as

$$h_c = \alpha_s L^{-0.2} P_{cyl}^{\ 0.8} T_{cyl}^{\ -0.73} \vartheta^{0.8} \tag{13}$$

where L is the instantaneous chamber height. The scaling factor, α_s is used for tuning of the coefficient to match specific engine geometry (α_s = 1.2 [46]). The instantaneous characteristic velocity, ϑ is

$$\vartheta = d\bar{S}_P \tag{14}$$

where $\bar{S}_P$ is the mean piston speed, d = 6.18 during gas exchange period and d = 2.28 for the closed part of the cycle [46]. Modified Woschni's correlation with constants listed in [49, 50] is used to calculate heat transfer coefficient for SI operating points. The in-cylinder gas temperature is calculated by solving energy equation using ideal gas law [43, 51] as

$$\frac{dT_{cyl}}{d\theta} = \frac{\sum \frac{dm_i}{d\theta}\left(h_i - u_i\right) + \frac{dQ_{cool}}{d\theta} - \frac{dQ_{HR}}{d\theta} - P\frac{dV}{d\theta}}{m_{cyl}C_v} \tag{15}$$

where $\frac{dm_i}{d\theta}$, h_i, and u_i are the mass flow rate, enthalpy and internal energy of the gas entering or leaving the cylinder respectively. The in-cylinder mass, m_{cyl} is obtained by solving conservation of mass [43, 51]. A one dimensional quasi steady compressible flow model is used to calculate mass flow rates through the intake and exhaust valves during induction and exhaust strokes [51]. Finally, the amount of injected fuel energy lost to the exhaust, Q_{exh} is calculated from an energy balance (see Figure 1) as

$$\begin{aligned} Q_{exh} = m_f Q_{LHV} - Q_{cool} - W_{friction} \\ - W_{brake} - Q_{IC} - W_{Pumping} \end{aligned} \tag{16}$$

The exhaust heat loss amount can be calculated based on the measured exhaust gas temperature [52], however, the sensor measurements are slow for cycle by cycle energy distribution analysis [53].

HCCI-CHP Exergy Analysis

A schematic of a CHP unit with HCCI engine is shown in Figure 2. The air/fuel mixture is burned in combustion chamber in HCCI mode and exhaust gas flow is used for the intake charge heating. Since only part of the fuel energy released during combustion is converted to the mechanical work, there is potential to recover the rest of the released heat. The HCCI energy balance including heat loss to the exhaust gas and cooling water was detailed in previous section. The heat from the lube oil, cooling water and exhaust gas can be recovered using intermediate heat exchangers as shown in Figure 2.

The brake thermal efficiency is the engine first law efficiency and indicates the fraction of the injected fuel energy turned into useful work. The second law efficiency however is a comparison of the system's thermal efficiency to the maximum possible efficiency [54]. From this point of view, exergy analysis is more useful for engine heat lost recovery analysis to understand the relative contribution of different loss mechanisms that result in performance reduction of engine. The theoretical maximum useful work that a system can produce is called exergy [54] and is calculated as

$$X = Q\left(1 - \frac{T_0}{T}\right) \tag{17}$$

FIGURE 2 HCCI engine flow diagram for a micro CHP unit

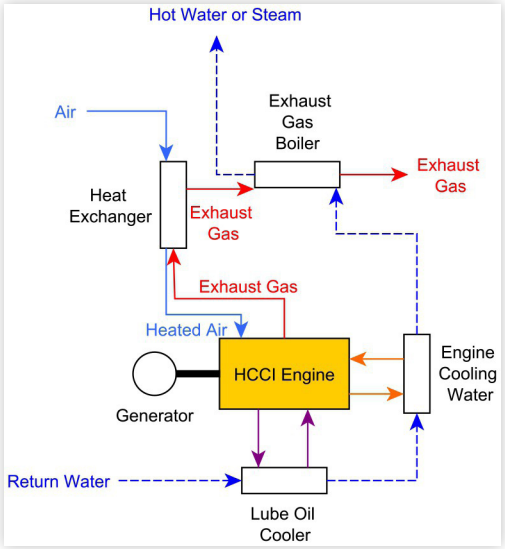

where Q, T_0 and T are the waste heat, ambient temperature and the waste heat temperature respectively ($T_0 = 25°C$). The exergy efficiency is the ratio of the exergy content of an energy source to the exergy content of the fuel [52] and is calculated as

$$\eta = \frac{X}{m_f x_f} \tag{18}$$

where x_f is the fuel exergy [55].

The exergy efficiency of the exhaust gas, η_{exh} is calculated as

$$\eta_{exh} = \frac{Q_{exh,CHP}\left(1 - \frac{T_0}{T_{exh}}\right)}{m_f x_f} \tag{19}$$

where T_{exh} is the measured exhaust gas temperature, and $Q_{exh,\,CHP}$ is calculated as

$$Q_{exh,CHP} = Q_{exh} - \frac{1}{\epsilon} m_{air} C_{p,air}\left(T_{Intake} - T_{Amb}\right) \tag{20}$$

where Q_{exh} is calculated from eqn. 16. The m_{air}, $C_{p,\,air}$, T_{Amb}, and T_{Intake} are the air mass per cycle heated by the intake heater (see Figure 2), specific heat ratio at constant pressure ($C_{p,air} = 1.006\ \frac{\text{kJ}}{\text{kg.K}}$), ambient temperature and intake manifold temperature after heating respectively. The effectiveness of the heat exchanger, ϵ is assumed to be constant ($\epsilon = 0.6$) [56].The second term in the right hand side of eqn. 20 is zero for SI engine exergy analysis as no intake heating is required. Next, the coolant exergy efficiency, η_{cool} is calculated as

$$\eta_{cool} = \frac{Q_{cool}\left(1 - \frac{T_0}{T_{cool}}\right)}{m_f x_f} \tag{21}$$

where Q_{cool} is calculated from eqn. 11 and T_{cool} is the coolant temperature.

For CHP system analysis, the first and second law efficiencies are needed. The first law efficiency of a CHP system is calculated [52] as

$$\eta_I = \frac{W_{el} + Q_{cool} + Q_{exh,CHP}}{m_f LHV_f} \tag{22}$$

where W_{el} is electric work that is obtained by coupling the engine to a generator. The electric generator efficiency is assumed to be 0.9 [1, 52] and the electric work is calculated as $W_{el} = 0.9 W_{brake}$.

The second law efficiency of a CHP system, η_{II} is defined [52] as

$$\eta_{II} = \frac{W_{el} + X_{cool} + X_{exh}}{m_f x_f} \tag{23}$$

where X_{cool} and X_{exh} are the coolant and exhaust exergies respectively and are calculated from eqn. 17. Finally, the power to heat ratio of a CHP system is calculated [1] as

$$\alpha = \frac{W_{el}}{Q_{cool} + Q_{exh,CHP}} \tag{24}$$

The power to heat ratio gives information about the quality of the CHP unit and the CHP potential for specific application is determined with this factor. Power to heat ratio values between 0.5 and 1.2 for existing micro CHP units integrated with internal combustion engines are recommended [1]. The cogeneration potential for each application depends on the heat load and power to heat ratio values. More low cost electricity can be produced at high power to heat ratios [1, 57, 58].

Combustion efficiency in HCCI engines is lower than other prime movers including turbines, SI and Diesel engines and incomplete combustion is one major source of energy losses in HCCI engines [27, 59, 60, 61, 62]. A new parameter is then defined for HCCI energy distribution analysis as

$$\beta = \frac{W_{el}}{Q_{cool} + Q_{exh,CHP} + Q_{IC}} \tag{25}$$

where β is the power to energy loss ratio.

Experimental Results and Analysis

HCCI Energy and Exergy Distribution

Measured pressure traces of HCCI engine for different SNVOs at constant fueling rate are shown in Figure 3. As shown in this figure, SNVO duration affects HCCI combustion, rate of pressure rise and maximum in-cylinder pressure. Energy distribution of the single cylinder HCCI engine with VVT is performed based on 35 steady state measured points listed in Table 2. The operating points are far from misfire as Indicated Mean Effective Pressure (IMEP) is positive [43] (see Figure 4(a)) and the combustion is stable as Coefficient of Variation (COV) of IMEP is below 3% [46, 63] for all operating points shown in Figure 4(b). The engine energy distribution is mainly detailed

FIGURE 3 Measured HCCI engine cylinder pressure traces [$\text{Em}_{\text{finj}} = 0.45\ \frac{\text{kJ}}{\text{Cycle}}$, n = 815 RPM]

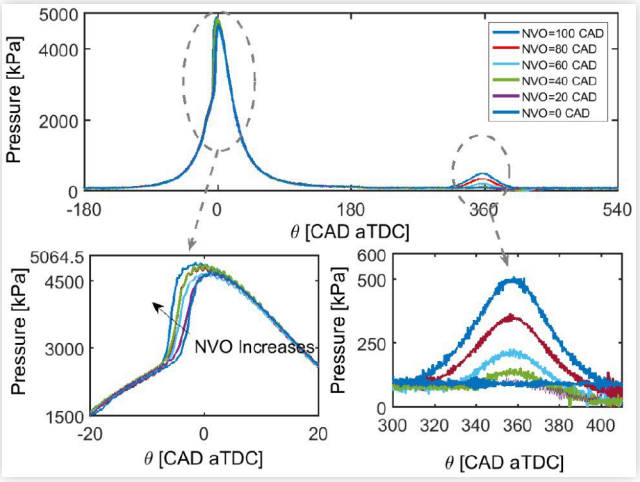

FIGURE 4 SNVO effects on (a) IMEP and (b) COV of IMEP at constant injected fuel energies

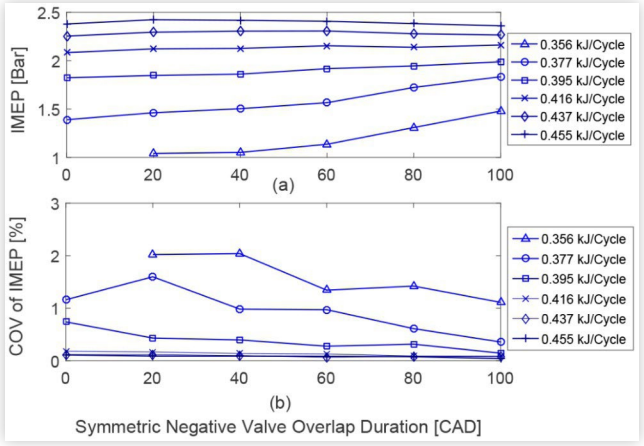

at low loads as efficient engine performance is necessary for fuel saving [26].

Only part of injected fuel energy is converted into the brake work (see Figure 1) and brake thermal efficiency is used to define the fraction of the injected fuel energy turned into the useful work. Brake thermal efficiency as a function of SNVO for several injected fuel energies is shown in Figure 5(a). Brake thermal efficiency increases at low injected fuel energies with increasing SNVO duration. Combustion timing advances with increase in SNVO duration as shown in Figure 5(b). Combustion timing is the crank angle of fifty percent fuel mass fraction burned in this work. The expansion ratio increases with the advanced combustion timing and the brake thermal efficiency is improved (see Figure 6 for $\mathrm{Em_{finj}} = 0.395 \ \frac{\mathrm{kJ}}{\mathrm{Cycle}}$). At high injected fuel energies, brake thermal efficiency is almost constant. For these operating points, combustion timing is advanced to before Top Dead Center (TDC) which increases the compression work. The increased compression work cancels the increased expansion work and the brake thermal efficiency remains almost constant (see Figure 5(a)).

FIGURE 5 SNVO effects on (a) the brake thermal efficiency and (b) combustion timing at constant injected fuel energies

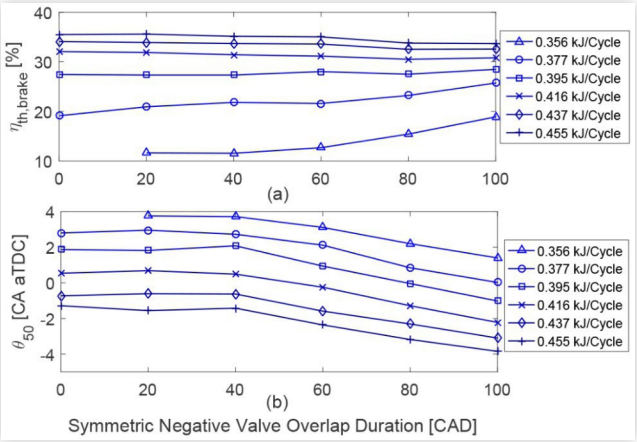

FIGURE 6 SNVO effects on (a) in-cylinder pressure, (b) cycle temperature, and (c) rate of heat release [$\mathrm{Em_{finj}} = 0.395 \ \frac{\mathrm{kJ}}{\mathrm{Cycle}}$, n = 819 RPM]

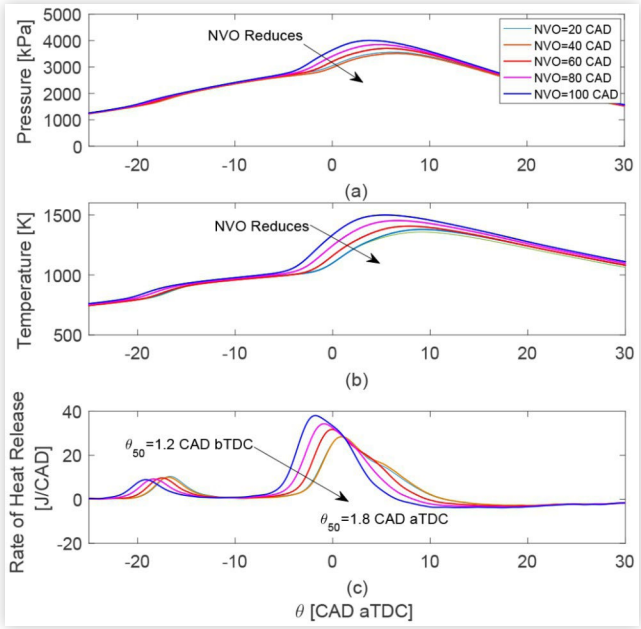

The effects of SNVO duration on the fraction of the injected fuel energy lost to the exhaust due to incomplete combustion is shown in Figure 7(a). At low injected fuel energies, combustion efficiency is improved with increase in SNVO duration. Combustion timing is advanced with increase in SNVO duration and mixture has enough time to completely burn and reactions are quenched later. At higher SNVO durations, more residual gas is trapped and it gives the unburned HC and CO remaining from the previous cycle a second chance to react. The peak cycle temperature increases with advanced combustion timing and improved combustion efficiency as shown in Figure 7(b). Combustion efficiency at high injected fuel energies is high and effects of SNVO duration on combustion efficiency is negligible. Figure 7(b) confirms this as the peak cycle temperature increases at lower rates with increased SNVO.

The waste heat recovery from the coolant and exhaust improves the engine fuel efficiency. About one-third of the injected fuel energy is lost to the exhaust with additional 11-12% losses to the coolant. The fraction of the injected fuel energy lost to the coolant slightly increases with increase in SNVO duration as shown in Figure 8(a). Combustion timing is advanced and the cycle temperature is increased when SNVO increases at constant injected fuel energies (see Figures 6(b) and 7(b)). The effects of SNVO duration on the fraction of the injected fuel energy lost to the exhaust is shown in Figure 8(b). The fraction of the fuel energy lost to the exhaust increases with increase in SNVO duration. Combustion efficiency improves and combustion timing advances with an increase in SNVO duration. The advanced combustion timing and higher combustion efficiencies increase the exhaust gas temperature and exhaust loses.

FIGURE 7 (a) Fraction of the injected fuel energy lost due to incomplete combustion and (b) Peak cycle temperature versus SNVO duration at constant injected fuel energies

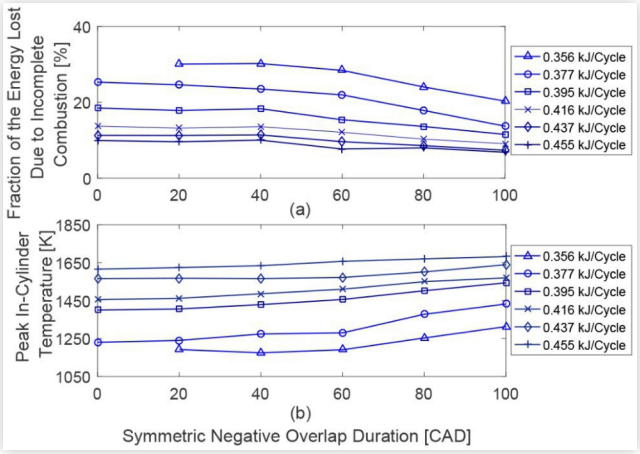

FIGURE 8 SNVO effects on the fraction of the injected fuel energy lost to the (a) coolant and (b) exhaust at constant injected fuel energies

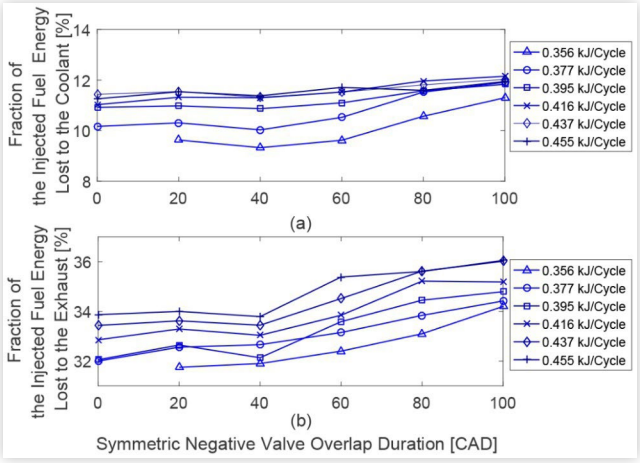

FIGURE 9 SNVO effects on the (a) exhaust gas exergy efficiency and (b) coolant exergy efficiency at constant injected fuel energies

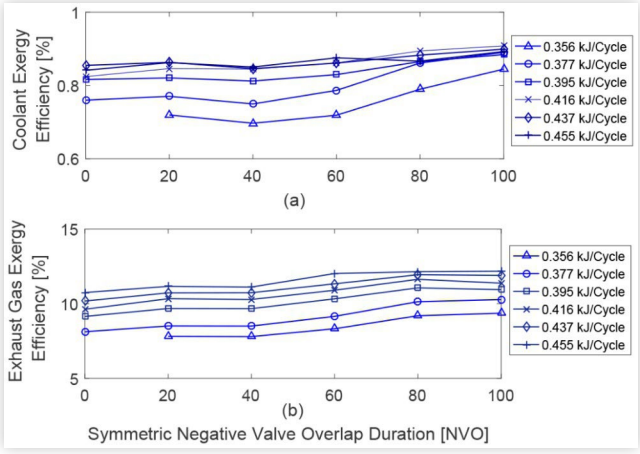

The quality of the waste heat flows are evaluated with the calculation of the exhaust and coolant exergy efficiencies. The coolant exergy efficiency is below 1% for all operating points as shown in Figure 9(a). The coolant exergy efficiency increases with an increase in SNVO duration as the fraction of the injected fuel energy lost to the coolant is increased with advanced combustion timing and improved combustion efficiency. Effects of SNVO duration on exhaust gas exergy efficiency is shown in Figure 9(b). Exhaust gas exergy efficiency increases with increase in SNVO duration as the fraction of the injected fuel energy lost to the exhaust increases. The coolant exergy efficiency is negligible compared to the exhaust exergy efficiency. This is attributed to a much higher exhaust gas temperature compared to the coolant water temperature so the fraction of the fuel energy lost to the exhaust is higher than the fraction of the fuel energy wasted to the coolant.

The effects of SNVO duration on CHP first law efficiency is shown in Figure 10(a). The maximum first law efficiency is about twice the maximum brake thermal efficiency, indicating that engine waste heat recovery is potentially important. At low injected fuel energies, CHP first law efficiency increases with increase in SNVO duration as combustion efficiency is improved. The fraction of the injected fuel energy lost to the coolant and exhaust increases with improved combustion efficiency while brake work increases with advanced combustion timing. At high injected fuel energies, SNVO duration has negligible effects on CHP first law efficiency. The fraction of the fuel energy lost to the coolant and exhaust increases with increase in SNVO duration, however, the brake work slightly reduces as compression work is increased. The effects of SNVO duration on the CHP second law efficiency is shown in Figure 10(b). The second law efficiency is about 30% lower than the first law efficiency because the coolant and exhaust exergies are smaller compared to the amount of energy lost to the exhaust gas and cylinder walls. At low injected fuel energies, the second law efficiency improves with increase in SNVO duration. At high injected fuel energies, the brake work reduces with increase in SNVO duration, however, the coolant and exhaust exergies are increased. The increase in coolant and exhaust exergies cannot compensate the brake work reduction and the second law efficiency, η_{II}, deteriorates slightly.

The effects of SNVO duration on the CHP power to heat ratio is shown in Figure 11(a). The power to heat ratio improves with increase in SNVO duration at low injected fuel energies. At low injected fuel energies, brake work and heat losses to the coolant and exhaust are increased with increase in SNVO duration. The increase in brake work is higher compared to the increase in energy losses to the coolant and exhaust and the power to heat ratio is increased as a result. At high injected fuel energies, the power to heat ratio, α, reduces slightly with increase in SNVO duration. Brake work reduces with increase in compression work and the fraction of the fuel energy lost to the exhaust and coolant increases due to advanced combustion timing and higher combustion efficiencies. The calculated power to heat ratio values shown in Figure 11(a) are between 0.3 and 0.85 that is closed to the values reported for micro-CHP units integrated with gas turbines [1]. The effects of SNVO duration on CHP power to energy loss ratio is shown

FIGURE 10 SNVO effects on the (a) η_I, first law, and (b) η_{II}, second law CHP efficiency, at constant injected fuel energies

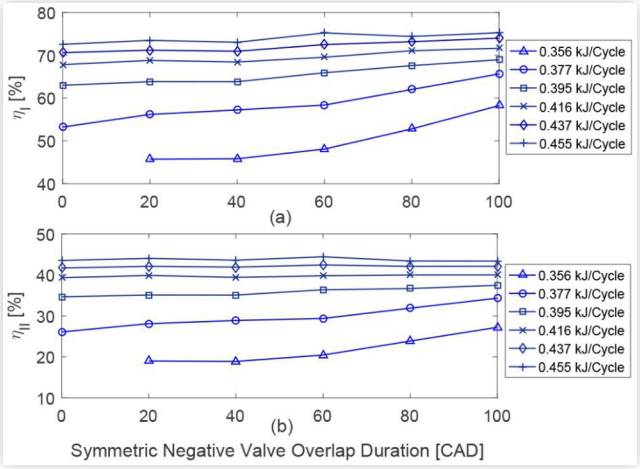

FIGURE 11 SNVO effects on the (a) α, power to heat ratio, and (b) β, power to energy loss ratio, at constant injected fuel energies

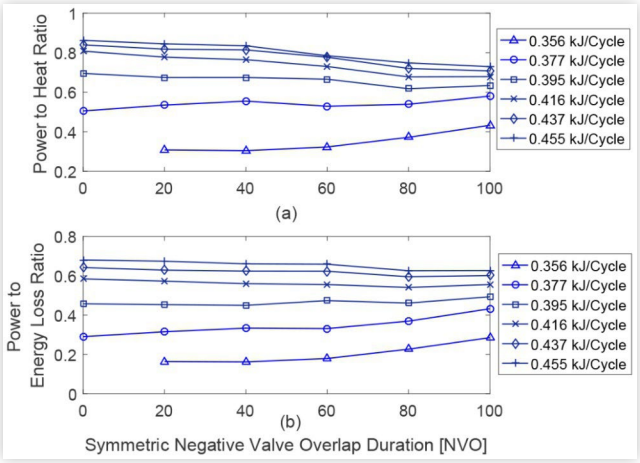

in Figure 11(b). At low injected fuel energies, power to energy loss ratio increases with an increase in SNVO duration, however, it is slightly reduced at high injected fuel energies. The power to energy loss ratio is about 20% less than power to heat ratio at high injected fuel energies. At low injected fuel energies, the power to heat ratio is twice the power to energy loss ratio. These results indicate that combustion efficiency has significant role in HCCI engine energy distribution.

Comparison with Si Combustion

The first and second law of thermodynamics are employed to compare the energy and exergy distributions of SI to HCCI experimentally. The combustion regime effects on fuel efficiency and the factors affecting exergy efficiencies are detailed. The comparison are made based on CFR experiments, with same compression ratio, injected fuel energy and engine speed. As detailed in Table 3, fuel octane number is varied by changing the iso-octane to n-heptane ratio for HCCI experiments. For SI experiments, spark timing is varied when the throttle is partially open. The fuel octane number and spark timing effects on the measured in-cylinder pressure and rate of heat release are shown in Figures 12 and 13. The energy distribution of each combustion mode at various fuel octane numbers and spark timings is shown in Figure 14.

HCCI can reach higher thermal efficiencies at same injected fuel energies compared to SI, although the combustion inefficiency of HCCI is 6.2% more than SI on average. This is mainly attributed to the low exhaust and heat transfer losses, and short burn duration, hence more fuel energy is converted to the output work. Similar to HCCI with VVT examined in Ricardo engine, SI and HCCI thermal efficiencies are improved by advancing combustion timing to TDC (see

FIGURE 12 HCCI CFR experiments - Fuel ON effects on (a) HCCI in-cylinder pressure, and (b) main HCCI rate of heat release [$\mathrm{Em_{finj}} = 0.65 \ \frac{\mathrm{kJ}}{\mathrm{Cycle}}$, n = 800 RPM]

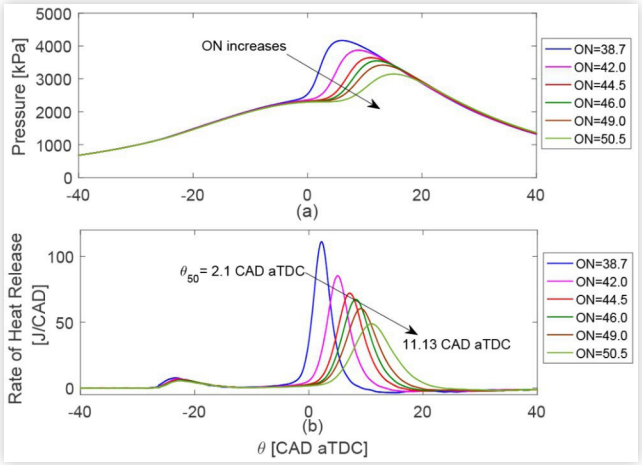

FIGURE 13 SI CFR experiments - spark timing effects on (a) SI in-cylinder pressure, and (b) SI rate of heat release [$\mathrm{Em_{finj}} = 0.65 \ \frac{\mathrm{kJ}}{\mathrm{Cycle}}$, n = 800 RPM]

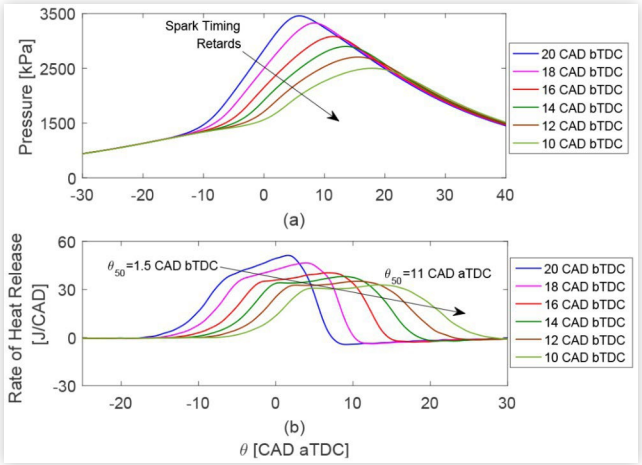

FIGURE 14 Energy distribution for (a) HCCI CFR at various ON, and (b) SI CFR at various spark timings

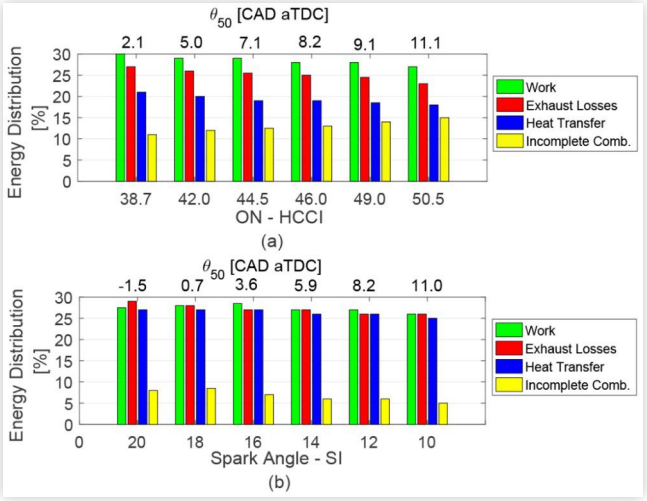

Figure 14). The fraction of the injected fuel energy lost to the coolant is higher for SI as combustion occurs in stoichiometric mixture and combustion temperature is higher compared to lean burn HCCI. For both SI and HCCI combustions, the heat losses to the coolant and exhaust increase with advanced combustion timing, and this is mainly attributed to the higher in-cylinder temperature at advanced combustion timings. The energy lost due to intake throttling is less than 5% of the injected fuel energy and it is calculated based on energy content of air mass flux in the intake manifold [54].

Exergy analysis is performed for further understanding of the HCCI and SI combustion regimes. The CHP first and second law analysis is performed and the power to heat and energy loss ratios are calculated (see Figure 15). Both CHP first and second law efficiencies are reduced with retarded combustion timing similar to HCCI combustion examined with VVT in Ricardo engine. The CHP first and second law efficiencies are higher for SI. This is mainly attributed to the higher SI combustion temperature and efficiency, and the fraction of fuel energy lost to the coolant and exhaust is high for SI. The HCCI power to heat ratio is higher compared to SI since HCCI has higher thermal efficiency and the fraction of fuel energy lost to the coolant and exhaust is lower due to low HCCI combustion temperature. The higher power to energy loss ratio in HCCI is mainly attributed to the higher HCCI thermal efficiency, the fraction of fuel energy turns into useful work.

FIGURE 15 Combustion timing effects on (a) η_I, first law, (b) η_{II}, second law, (c) α, power to heat ratio, and (d) β, power to energy loss ratio

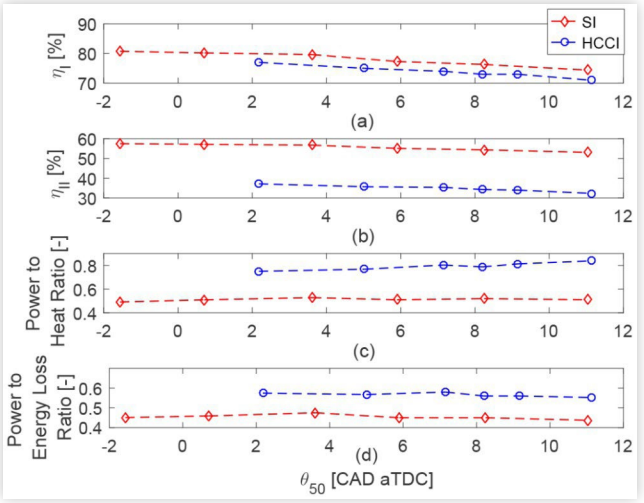

Conclusions

HCCI engine energy distribution analysis is performed based on 35 measured steady state points to characterize SNVO effects on the distribution of supplied fuel energy. Coolant and exhaust exergies are calculated for engine waste heat recovery analysis. The results indicate that VVT with SNVO is an effective actuator for combustion and CHP first and second law efficiency improvement, specifically at low injected fuel energies. Combustion efficiency has an important role in HCCI engine energy distribution and the CHP power to heat ratio is improved as combustion efficiency improves. Brake thermal efficiency is improved at higher combustion efficiencies for appropriate combustion timings. Incomplete combustion is one major source of energy losses in HCCI engines. Power to energy loss ratio is defined for energy distribution analysis in HCCI engines as it includes fraction of the fuel energy lost due to incomplete combustion. Higher power to energy loss ratios are obtained at higher combustion efficiencies where combustion timings are near TDC. The HCCI energy and exergy distribution is compared to SI using CHP first and second law efficiencies. The combustion timing affects both HCCI and SI energy distribution. The heat losses to the coolant and exhaust are higher for SI combustion due to its higher cycle temperature and combustion efficiency. SI demonstrates higher CHP first and second law efficiencies, while HCCI power to heat and energy loss ratios are higher due to its higher thermal efficiency. The results presented in this paper could provide a basis for the development of an HCCI engine based micro-CHP systems working at constant engine speed and varying loads with VVT.

References

1. Vuorinen, A., "*Planning of Optimal Power Systems*," (Vammala, Vammalan Kirjapaino Oy, 2009).
2. Beith, R., "*Small and Micro Combined Heat and Power (CHP) Systems: Advanced Design, Performance, Materials and Applications*," Woodhead Publishing Series in Energy: no. 18, (Cambridge/Philadelphia, Woodhead Pub., 2011).
3. Aceves, S.M., Martinez-Frias, J., and Reistad, G.M., "Analysis of Homogeneous Charge Compression Ignition (HCCI) Engines for Cogeneration Applications," *Journal of Energy Resources Technology* 128(1):16, 2006.

4. Zhao, H., "*HCCI and CAI Engines for the Automotive Industry*," (CRC Press, 2006).
5. Schramm, A., "Effects of Negative Valve Overlap on HCCI Combustion and its Use in the Control of HCCI Combustion Timing," Master's thesis, University of Alberta, 2014.
6. Williams, S., Hu, L.R., Nakazono, T., Ohtsubo, H. et al., "Oxidation Catalysts for Natural Gas Engine Operating under HCCI or SI Conditions," *SAE Int. J. Fuels Lubr.* 1(1):326-337, 2008, doi:10.4271/2008-01-0807.
7. Lu, X.-C., Chen, W., and Huang, Z., "A Fundamental Study on the Control of the HCCI Combustion and Emissions by Fuel Design Concept Combined with Controllable EGR. Part 2. Effect of Operating Conditions and EGR on HCCI Combustion," *Fuel* 84(9):1084-1092, 2005.
8. "CHP for Commercial Buildings: Fuel Cell, Engine, and Turbine Technologies for Cogeneration in Commercial, Institutional, and Municipal Buildings: Global Market Analysis and Forecasts," *PR Newswire*, 2015.
9. Stathopoulos, P. and Paschereit, C., "Retrofitting Micro Gas Turbines for Wet Operation. A Way to Increase Operational Flexibility in Distributed CHP Plants," *Applied Energy* 154:438-446, 2015.
10. "Catalog of CHP Technologies-Section 2. Technology Characterization-Reciprocating Internal Combustion Engines, Combined Heat and Power Partnership, U.S. Environmnetal Protection Agency," 3, 2015.
11. Saxena, S., Bedoya, I.D., Shah, N., and Phadke, A., "Understanding Loss Mechanisms and Identifying Areas of Improvement for HCCI Engines Using Detailed Exergy Analysis," *J. Eng. Gas Turbines Power*, no. GTP-13-110, 10, 2013.
12. Saxena, S., Shah, N., Bedoya, I., and Phadke, A., "Understanding Optimal Engine Operating Strategies for Gasoline-Fueled HCCI Engines Using Crank-Angle Resolved Exergy Analysis," *Applied Energy* 114(0):155-163, 2014.
13. Jafarmadar, S. and Javani, N., "Exergy Analysis of Natural Gas/DME Combustion in Homogeneous Charge Compression Ignition Engines (HCCI) Using Zero-Dimensional Model with Detailed Chemical Kinetics Mechanism," *International Journal of Exergy* 15(3):363, 2014.
14. Fatehi Ghahfarokhi, R., Khalilarya, S., and Ebrahimi, R., "Energy and Exergy Analyses of Homogeneous Charge Compression Ignition (HCCI) Engine," *Thermal Science* 17(1):107-117, 2013.
15. Sarabchi, N., Saray, R.K., and Mahmoudi, S., "Utilization of Waste Heat from a HCCI Engine in a Tri-Generation System," *Energy* 55:965-976, 2013.
16. Kobayashi, K., Sako, T., Sakaguchi, Y., Morimoto, S. et al., "Development of HCCI Natural Gas Engines," *Journal of Natural Gas Science and Engineering* 3(5):651-656, 2011.
17. Wagner, R.M., Briggs, T.E., Theiss, T.J., Singh, G. et al., "Defining Engine Efficiency Limits," *17th DEER Conference*, Detroit, 2011.
18. Mamalis, S. and Assanis, D.N., "Second-Law Analysis of Boosted HCCI Engines: Modeling Study," *Journal of Energy Engineering* 141(2):1-9, 2015.
19. Farrell, J.T., Stevens, J.G., and Weissman, W., "A Second Law Analysis of High Efficiency Low Emission Gasoline Engine Concepts," SAE Technical Paper 2006-01-0491, 2006, doi:10.4271/2006-01-0491.
20. Khaliq, A., Trivedi, S.K., and Dincer, I., "Investigation of a Wet Ethanol Operated HCCI Engine Based on First and Second Law Analyses," *Applied Thermal Engineering* 31(10):1621-1629, 2011.
21. Amjad, A., Saray, R.K., Mahmoudi, S., and Rahimi, A., "Availability Analysis of N-Heptane and Natural Gas Blends Combustion in HCCI Engines," *Energy* 36(12):6900-6909, 2011.
22. Djermouni, M. and Ouadha, A., "Thermodynamic Analysis of an HCCI Engine Based System Running on Natural Gas," *Energy Conversion and Management* 88(0):723-731, 2014.
23. Li, Y., Jia, M., Chang, Y., Kokjohn, S.L. et al., "Thermodynamic Energy and Exergy Analysis of Three Different Engine Combustion Regimes," *Applied Energy* 180:849-858, 2016.
24. Razmara, M., Bidarvatan, M., Shahbakhti, M., and Robinett, R.D., "Optimal Exergy-Based Control of Internal Combustion Engines," *Applied Energy* 183:1389-1403, 2016.
25. Kavuri, C., Paz, J., and Kokjohn, S.L., "A Comparison of Reactivity Controlled Compression Ignition (RCCI) and Gasoline Compression Ignition (GCI) Strategies at High Load, Low Speed Conditions," *Energy Conversion and Management* 127(Supplement C):324-341, 2016.
26. Ekoto, I., Wolk, B., and Northrop, W., "Energy Analysis of Low-Load Low-Temperature Gasoline Combustion with Auxiliary-Fueled Negative Valve Overlap," *SAE Int. J. Engines* 10(10):1238-1255, 2017, doi:10.4271/2017-01-0729.
27. Dernotte, J., Dec, J.E., and Ji, C., "Energy Distribution Analysis in Boosted HCCI-like/LTGC Engines-Understanding the Trade-Offs to Maximize the Thermal Efficiency," *SAE Int. J. Engines* 8:956-980, 2015, doi:10.4271/2015-01-0824.
28. Ravi, N., Liao, H.-H., Jungkunz, A.F., Widd, A. et al., "Model Predictive Control of HCCI Using Variable Valve Actuation and Fuel Injection," *Control Engineering Practice* 20(4):421-430, 2012; Special Section: *IFAC Symposium on Advanced Control of Chemical Processes -ADCHEM*, 2009, doi:10.1016/j.conengprac.2011.12.002.
29. Shaver, G., Roelle, M., and Gerdes, J., "Decoupled Control of Combustion Timing and Work Output in Residual-Affected HCCI Engines," *Proceedings of the 2005 American Control Conference*, vol. 6, 3871-3876, June 2005, doi:10.1109/ACC.2005.1470578.
30. Ebrahimi, K. and Koch, C.R., "Model Predictive Control for Combustion Timing and Load Control in HCCI Engines," SAE Technical Paper 2015-01-0822, 2015, doi:10.4271/2015-01-0822.
31. https://powergen.gepower.com/applications/chp.html.
32. Brammer, J. and Bridgwater, A., "The Influence of Feedstock Drying on the Performance and Economics of a Biomass Gasifier-Engine CHP System," *Biomass and Bioenergy* 22(4):271-281, 2002.
33. Onovwiona, H. and Ugursal, V., "Residential Cogeneration Systems: Review of the Current Technology," *Renewable and Sustainable Energy Reviews* 10(5):389-431, 2006.
34. Moran, A., Mago, P.J., and Chamra, L.M., "Thermoeconomic Modeling of Micro-CHP (Micro-Cooling, Heating, and

Power) for Small Commercial Applications," *International Journal of Energy Research* 32(9):808-823, 2008.

35. Míguez, J.L., Murillo, S., Porteiro, J., and López, L., "Feasibility of a New Domestic CHP Trigeneration with Heat Pump: I. Design and Development," *Applied Thermal Engineering* 24(10):1409-1419, 2004.
36. Talbi, M. and Agnew, B., "Energy Recovery from Diesel Engine Exhaust Gases for Performance Enhancement and Air Conditioning," *Applied Thermal Engineering* 22(6):693-702, 2002.
37. Abusoglu, A. and Kanoglu, M., "Exergetic and Thermoeconomic Analyses of Diesel Engine Powered Cogeneration: Part 1 Formulations," *Applied Thermal Engineering* 29(23):234-241, 2009.
38. Mostafavi, M. and Agnew, B., "Thermodynamic Analysis of Combined Diesel Engine and Absorption Refrigeration Unit-Naturally Aspirated Diesel Engine," *Applied Thermal Engineering* 17(5):471-478, 1997.
39. Pepermans, G., Driesen, J., Haeseldonckx, D., Belmans, R. et al., "Distributed Generation: Definition, Benefits and Issues," *Energy Policy* 33(6):787-798, 2005.
40. Seethaler, R., Mashkournia, M., Chladny, R.R., Zhao, J. et al., "Closed Loop Electromagnetic Valve Actuation Motion Control on a Single Cylinder Engine," SAE Technical Paper 2013-01-0594, 2013, doi:10.4271/2013-01-0594.
41. Slepicka, C., "Iterative Learning Control for Fuel Robust HCCI," M.Sc. thesis, University of Alberta, 2016.
42. Ebrahimi, K., Aliramezani, M., and Koch, C.R., "An HCCI Control Oriented Model that Includes Combustion Efficiency," *IFAC-Papers OnLine* 49(11):327-332, 2016; *8th IFAC Symposium on Advances in Automotive Control AAC 2016Norrkping*, Sweden, 20-23 June 2016.
43. Heywood, J.B et al., "*Internal Combustion Engine Fundamentals*, vol. 930," McGraw-Hill, New York, 1988.
44. Kirchen, P.N., "Thermokinetic Modelling of the HCCI Cycle," Master's thesis, University of Alberta, 2004.
45. Marvin Jr, C.F., "*Combustion Time in the Engine Cylinder and Its Effect on Engine Performance*," 1928.
46. Shahbahkti, M., "Modeling and Experimental Study of an HCCI Engine for Combustion Timing Control," PhD thesis, University of Alberta, 2009.
47. Souder, J.S., "Closed-Loop Control of a Multi-Cylinder HCCI Engine," PhD thesis, University of California, Berkeley, 2004.
48. Chang, J., Güralp, O., Filipi, Z., Assanis, D.N. et al., "New Heat Transfer Correlation for an HCCI Engine Derived from Measurements of Instantaneous Surface Heat Flux," SAE Technical Paper 2004-01-2996, 2004, doi:10.4271/2004-01-2996.
49. Shayler, P., May, S., and Ma, T., "The Determination of Heat Transfer from the Combustion Chambers of SI Engines," SAE Technical Paper 931131, 1993, doi:10.4271/931131.
50. Abedin, M., Masjuki, H., Kalam, M., Sanjid, A. et al., "Energy Balance of Internal Combustion Engines Using Alternative Fuels," *Renewable and Sustainable Energy Reviews* 26:20-33, 2013.
51. Assanis, D.N. and Heywood, J.B., "Development and Use of a Computer Simulation of the Turbocompounded Diesel System for Engine Performance and Component Heat Transfer Studies," SAE Technical Paper 860329, 1986, doi:10.4271/860329.
52. Magno, A., Mancaruso, E., and Vaglieco, B.M., "Effects of a Biodiesel Blend on Energy Distribution and Exhaust Emissions of a Small CI Engine," *Energy Conversion and Management* 96(0):72-80, 2015.
53. Firoozabadi, M.D., Shahbakhti, M., Koch, C., and Jazayeri, S., "Thermodynamic Control-Oriented Modeling of Cycle-to-Cycle Exhaust Gas Temperature in an HCCI Engine," *Applied Energy* 110(0):236-243, 2013.
54. Cengel, Y.A. and Boles, M.A., "*Thermodynamics: An Engineering Approach*, McGraw-Hill Series in Mechanical Engineering," (Boston, McGraw-Hill Higher Education, 2006).
55. Szybist, J.P., Chakravathy, K., and Daw, C.S., "Analysis of the Impact of Selected Fuel Thermochemical Properties on Internal Combustion Engine Efficiency," *Energy & Fuels* 26(5):2798-2810, 2012.
56. Saxena, S., Vuilleumier, D., Kozarac, D., Krieck, M. et al., "Optimal Operating Conditions for Wet Ethanol in a HCCI Engine Using Exhaust Gas Heat Recovery," *Applied Energy* 116:269-277, 2014.
57. Savola, T. and Fogelholm, C.-J., "Increased Power to Heat Ratio of Small Scale CHP Plants Using Biomass Fuels and Natural Gas," *Energy Conversion and Management* 47(1819):3105-3118, 2006.
58. Frangopoulos, C.A., "A Method to Determine the Power to Heat Ratio, the Cogenerated Electricity and the Primary Energy Savings of Cogeneration Systems after the European Directive," *Energy* 45(1):52-61, 2012.
59. Jun, D. and Iida, N., "A Study of High Combustion Efficiency and Low CO Emission in a Natural Gas HCCI Engine," SAE Technical Paper 2004-01-1974, 2004.
60. Lefebvre, A., "Fuel Effects on Gas Turbine Combustion-Ignition, Stability, and Combustion Efficiency," *Am. Soc. Mech. Eng.*, (Pap.); (United States), 1984.
61. Paepe, M.D., DHerdt, P., and Mertens, D., "Micro-CHP Systems for Residential Applications," *Energy Conversion and Management* 47(1819):3435-3446, 2006.
62. Bishop, R.P., "*Combustion Efficiency in Internal Combustion Engines*," 1985.
63. Bahri, B., Aziz, A.A., Shahbakhti, M., and Said, M.F.M., "Understanding and Detecting Misfire in an HCCI Engine Fuelled with Ethanol," *Applied Energy* 108(Supplement C):24-33, 2013.

ISSN 0148-7191